AERODYNAMICS AND HEAT EXCHANGE PROCESSES OF AIRCRAFT

NUMERICAL AND EXPERIMENTAL INVESTIGATION OF THE HYPERSONIC FLOW STRUCTURE IN A COMPLEX FLAT DUCT

M.A. Kotov, **I.A. Kryukov**, **L.B. Ruleva**,
S.I. Solodovnikov, **S.T. Surzhikov**

Institute for Problems in Mechanics of the Russian Academy of Sciences
e-mail: mikhail_kotov88@mail.ru; kryukov@ipmnet.ru; ruleva@ipmnet.ru; sis63@yandex.ru; surg@ipmnet.ru

Experimental and numerical investigation was performed to determine the hypersonic flow structure in a complex flat duct simulating the air intake and flow passage in a hypersonic ramjet. The testing setup is described in detail. Mach 7 and Mach 4.5 air flows are studied by means of high-speed digital video cameras in the flat ducts formed by sharp and blunt-nose wedges. The duct internal surface was either smooth or had trapezoid cavities similar to flameholders in a hypersonic ramjet engine combustion chamber. The numerical simulation was conducted with the software (computer code) integrating the Navier-Stokes equation system. The comparison of testing and computational data proves that numerical simulation can provide accurate description of the experimental flow structure. The numerical and experimental results clearly present hypersonic flow field structure in complex configuration ducts. Simultaneous computational and experimental investigation enhances the reliability of the aerodynamic data obtained.

Keywords: shock tube, experimental investigation, hypersonic flows, shockwave mathematical modelling, gas dynamics equations, compressible Navier–Stokes equations, finite volume approach.

Problem description. Intensive physical processes near the surface of the aerospace and hypersonic aircraft (HA) justify the investigation of high-speed and high-temperature gas flows normally accompanied by a multitude of non-linearly related physical processes, which stipulates a complex approach drawing both on the physical experiment and corresponding computational models.

Such investigations require physical processes data obtained from (geometrically-) scaled model testing in a shock tube [1]. These setups are a fairly convenient tool for a wide range of aerodynamics and physical dynamics problems and enable validation of numerical methods. Short duration of gas dynamics processes in the shock tube working path which complicates measurements is canceled out by low-inertia sensors, noncontact measuring equipment (shadow column devices, interferometers) [2–4] based on optical instruments and new generation high-speed recording and processing equipment.

This paper presents the results of the experimental and numerical investigation of shockwave patterns as a result of hypersonic flow past HA elements. Aerodynamic models of the following flat duct types were studied:

- different-thickness sharp wedges;
- same-thickness sharp wedges with internal trapezoid cavities;
- same-thickness blunt nose wedges with internal trapezoid cavities.

There exist various classifications [5, 6] of gas dynamic experimental setups ranging from transonic to hypersonic velocities. Since research in this field covers fundamental investigation of HA aerodynamic performance (including hypersonic ramjet propulsion unit), particular attention should be paid to the measurement accuracy issues in short duration aerodynamic tests [6]. The research in question used the hypersonic shock tube at the Institute of Problems in Mechanics of RAS [7–10] which operates on the impulse-type wind tunnel principle and enables supersonic and hypersonic flow investigation for the aircraft mockups and their individual structural elements [1].

Consideration of hypersonic patterns interaction in various duct configurations is preceded by the analysis of the test data on shockwave flow pattern in the shock tube. It is demonstrated that the multiple passage of the shock waves through the shock tube enabled creation of several quasi steady hypersonic flow modes.

The shockwave interaction pattern for the models tested was reproduced in numerical experiments using proprietary computer code.

Experimental setup description. The hypersonic shock tube was designed for the experimental investigation of aerodynamic flow field structure around scaled models at supersonic and hypersonic velocities [7–10]. The overall length of the installation is 14.5. . . 22 m, which can be varied depending on the desired flow parameters. It comprises three to five segments. High pressure chamber (HPC) is made out of corrosion-resistant steel, is 1.97 m in length and 8 cm in cross section diameter. This segment operates with room temperature gases at the pressure up to 22 bar. Low pressure chamber (LPC) is 7.35 in length and has the same cross section diameter. LPC is made out of corrosion-resistant steel and is separated from the HPC by a membrane. These segments can be elongated by 7.5 m with extra segments.

A nozzle unit is installed at the end of the LPC with an aluminium diaphragm at its entrance. This diaphragm is ruptured by the initial shockwave, thus the flow expands through the nozzle into the receiver. The models tested are placed in the receiver and can be positioned at the nozzle exit or at some distance from it.

The hypersonic shock tube is equipped with piezo electric sensors to record shockwave interaction in the course of the experiment. The setup is shown schematically in Fig. 1. One sensor (A) is placed at the beginning of the HPC and is used to identify the compression/rare faction waves hitting the section wall. The other sensors (B, C) are positioned in the middle and

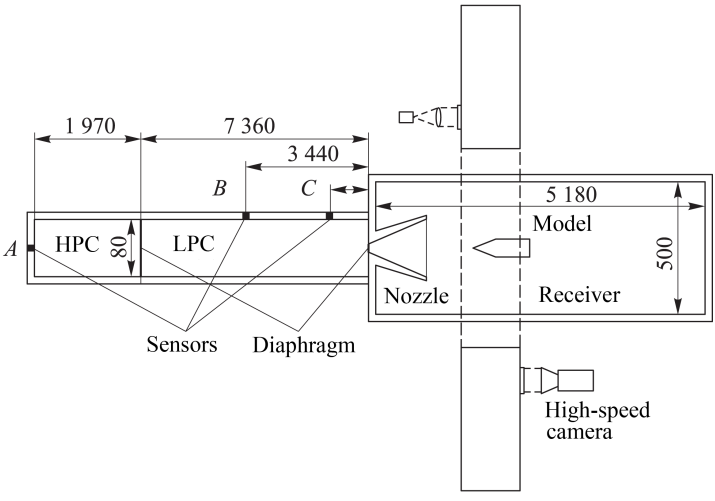

Fig. 1. Schematic view of the testing setup

at the end of the HPC in order to trigger the recording equipment, measure the shockwave velocity, detect the pressure change and shockwave pattern history. All sensors are connected to a personal computer via the analog-digital transducer.

Optical investigation of the flow around the models is conducted via flat illuminators 260 mm in diameter. Shadow column instruments (Tepler devices ИАБ-451 were used in this case) provide photo and video data on the shockwave and boundary layers behavior in the area under investigation. These data were recorded by means of digital high-speed video cameras with several thousand shots per second speed. The cameras were activated by pressure sensors.

The desired rarefaction level in the testing setup segments is achieved by means of two turbomolecular oil-free vacuum pumps. The high pressure and low pressure chambers are separated by a copper diaphragm. A system of blades was used for the uniform and rapid opening of the diaphragm. The low pressure chamber and the receiver are separated by a thin aluminium membrane positioned at the nozzle unit entrance.

The shock tube produces Mach 7.0 hypersonic flows in the receiver segment. A number of experiments were conducted to simulate the flow in the ramjet air intake. The scaled models have wedge-shaped elements, some of them blunted. Special cavities on the surface simulate flame holders in real ramjet ducts [11].

Shock tube experiment results. Typical readings for pressure sensors during the experiment are presented in Fig. 2, 3. In this case, the driver gas is air at 20 bar pressure; the driven gas is air at 100 mbar pressure. The oscillograph patterns log the pressure changes at 10 cm distance to the nozzle entrance (sensor *C*, Fig. 1). The first jump (*1*, Fig. 2) indicates the

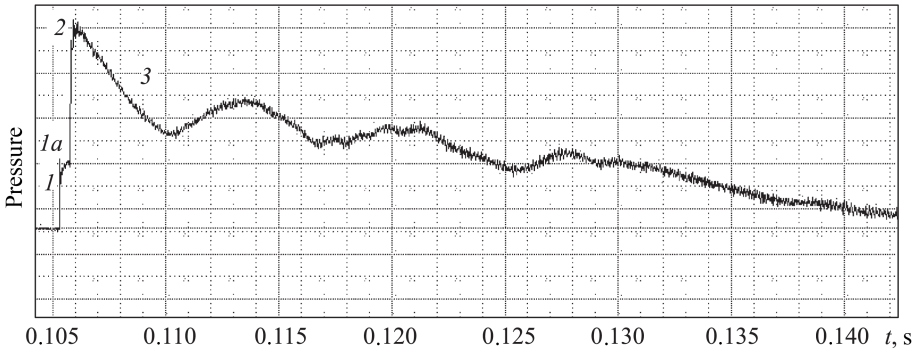

Fig. 2. Pressure sensor readings at the nozzle unit entrance

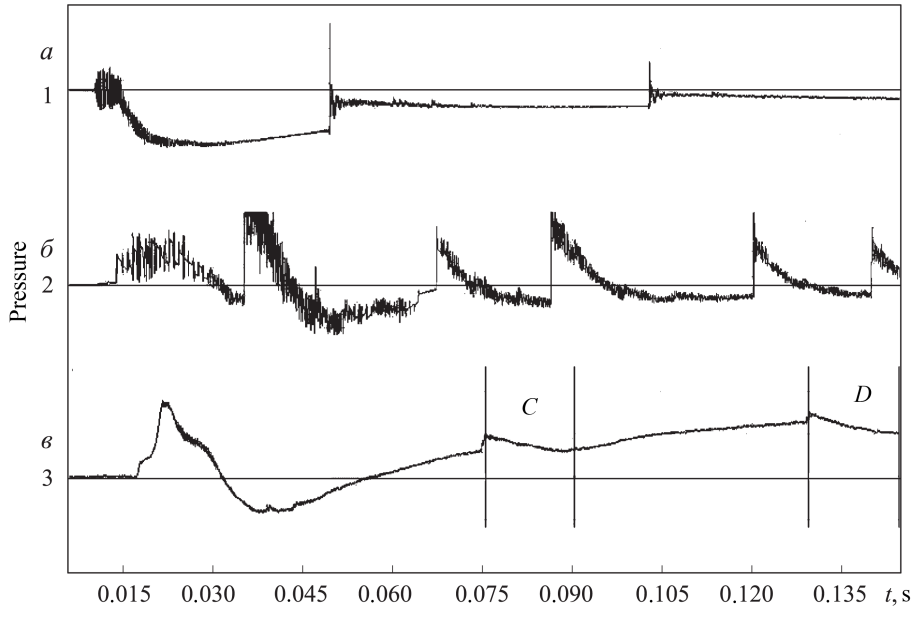

Fig. 3. Pressure sensor readings in the shock tube

initial shockwave. At approximately 300 ms before the shockwave reflected from the right end wall (fragment *1a* in the oscillogram, Fig. 2) the gas following the head shockwave passes through the cross-section where the sensor is located. The phase in question is closely studied by means of numerical simulation in [10], where the structure of the flow following the reflected shockwave front was investigated under shock tube tests conditions. The subsequent sharp increase in pressure (*2*, Fig. 2) and the smooth decrease (*3*, Fig. 3) to the fluctuating values indicate the shock wave reflected from the nozzle end wall and the quasi steady flow parameters (about 10 ms) before the rarefaction wave.

The oscillograph patterns of the pressure sensors located in various areas of the shock tube are presented in Fig. 3. The test initial conditions were the same as in Fig. 2. The top graph indicates the pressure for the

HPC end wall (the *A* sensor is positioned flush with the left end wall of the HPC). A short period of time after the diaphragm opening a fall in pressure is observed which results from the rarefaction waves fan. Further jumps indicate perturbation reflected from the LPC end wall and its subsequent reflection from the HPC end wall.

The next two oscillograph patterns (Fig. 3 *b, c*, sensors *B*, *C* in Fig. 1) demonstrate changing pressure in the LPC (the middle and the end part of the segment). It is visible that the pressure in the middle part of the segment increases when the initial shockwave passes through sensor *B*. After approximately 3.3 ms sensor *C* (lower graph) displays reaction to this perturbation. The further readings of this sensor are similar to the ones described above (Fig. 2). The next jump in the oscillograph pattern of sensor *B* (Fig. 1) in the middle of the LPC corresponds to the reflected shockwave.

The data in Fig. 3 display shockwave interaction caused by the multiple re-reflection of rarefaction jumps within the shock tube volume. Due to this behavior several time intervals which can be regarded as quasi steady can be identified. Some of these intervals being several milliseconds long can be used for measurements.

Results of the experiments on hypersonic flow in the receiver. Shadow images of the driven gas flow around the models were recorded by high-speed video cameras and Schlieren optical system. Fig. 4 presents hypersonic flow near the 10° wedge and 5° semi-wedge. The initial conditions were the following: driven gas in LPC was air at 1 mbar pressure, the driver gas in HPC was air at 36 bar pressure, pressure in the receiver segment was 4. . . 10 mbar. The 10° wedge was positioned so that its central longitudinal axis and the nozzle symmetry axis coincided. The distance between the models was 15 mm.

The air flow with the constant Mach number (Fig. 4 *a*) lasts for about 15 ms. Then the flow parameters at the nozzle entrance change, with

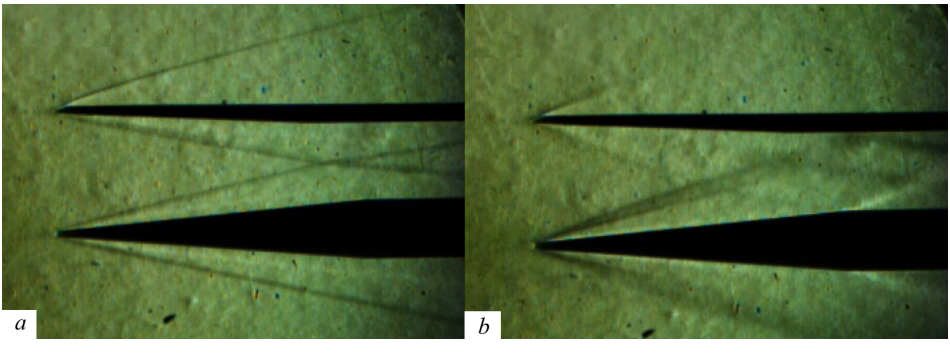

Fig. 4. Hypersonic air flow (*a*) and its subsequent perturbation (*b*); images from the shadow video sequence

the flow pattern changing as well (Fig. 4 *b*). Experimental angle of the shockwave front deflection from the wedge ($\alpha = 13^\circ$, $\beta = 5^\circ$ for the lower 10° wedge) was used to calculate the Mach number for the ram air according to the formula [5]

$$\mathrm{M} = \left(\sin^2 \alpha - \frac{\gamma - 1}{2} \cdot \frac{\sin \alpha \sin \beta}{\cos(\alpha - \beta)} \right)^{-1/2}.$$

Mach number for the lower 10° wedge was 7.09 (Fig. 4 *a*). The flow parameter values for a semi wedge can be estimated with lesser accuracy (a greater angle of shockwave deflection from its upper surface can be observed), which is caused by the model being at a distance from the nozzle symmetry axis.

Under similar initial conditions flow tests were conducted on models simulating air intake of a pespective HA. These models were represented by two blunt-nose 10° wedges with 1.5 mm bluntness radius and 10 mm thickness. In order to investigate shockwave interaction in a complex configuration duct simulating flame holders in the gas dynamic passage, the models were provided with special cavities, 3 mm deep. The models were positioned symmetrically to the nozzle axis at 2 cm distance from each other. This was done to ensure homogeneous field flow parameters between the models. Fig. 5 presents shadow images of the test.

The process presented in Fig. 5, *a* is caused by the first stage of the driven gas expansion through the nozzle on to the model, which is optimally suited for the high-speed test, since at this period the flow parameters from the nozzle unit are approximately constant, with $\mathrm{M} = 7$. At the shadow video it is experimentally observed for 15 ms.

After the rarefaction waves fan and the contact surface of the driver gas hit the LPC right end wall, the pressure at the nozzle entrance decreases and the flow parameters start to fluctuate significantly. This perturbation is shown in Fig. 5 *b*, it lasts for about 5. . . 7 ms. After that the shockwave interaction process in the shock tube is determined by multiple passes and rarefactions of shock waves between LPC and HPC sidewalls. However, it is possible to identify time intervals in which gas parameters at the nozzle entrance change insignificantly. Such type periods can be directly connected and numerically characterized with the data presented in the oscillograph pattern (Fig. 3 *c*). In particular, fragment *C* in the oscillograph pattern corresponds to the second, lower velocity quazi steady flow mode presented in 5 c. The duration of this period is $t_c \approx 30$ ms, $\mathrm{M} = 4.5$.

In the course of the experiments the third quazi steady flow stage ($\mathrm{M} \cong 3$) was identified which corresponded to fragment *D* of the oscillograph pattern in Fig. 3.

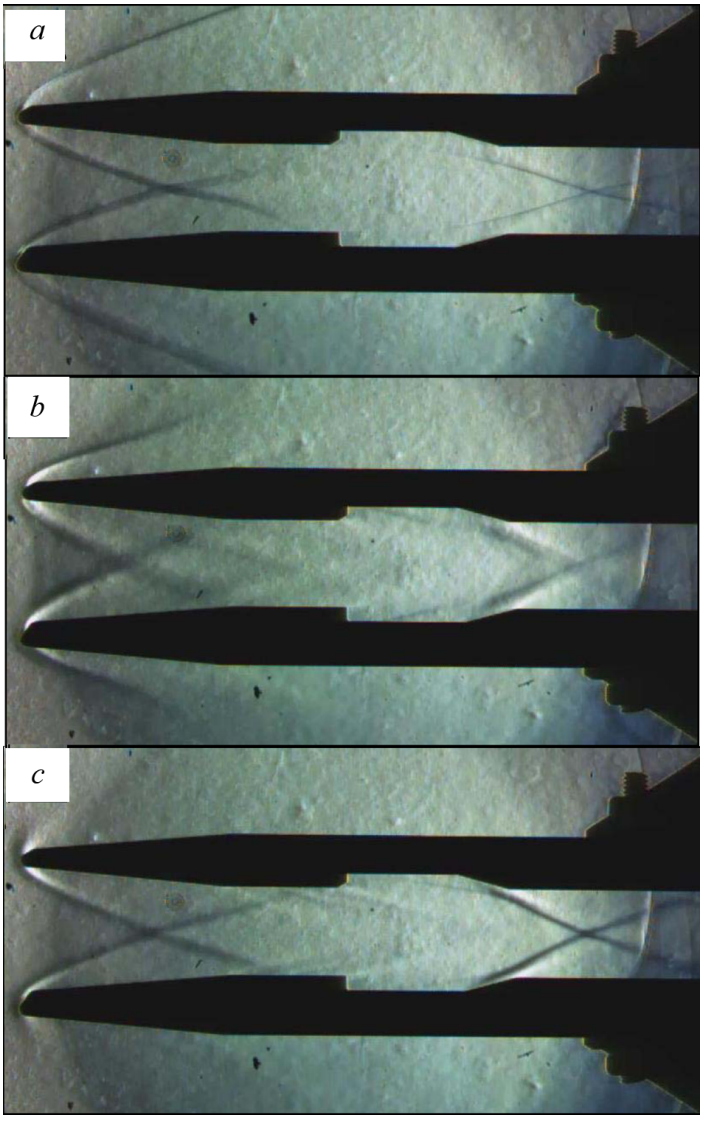

Fig. 5. Shockwave structure around two blunt-nose wedges; shadow-column images of the test

In order to determine the flow velocity characteristics more accurately and adjust the Schlieren equipment, experiments with sharp wedges were conducted similar to the ones described above. The positioning of the models also remained unchanged. The results are shown in Fig. 6.

The photos are in order corresponding to the order in Fig. 5. The steady parameters flow approaches the model (Fig. 6 *a*). It is replaced by perturbations (Fig. 6 *b*), which are followed by the quazi steady flow process (Fig. 6 *c*).

The comparison of the shockwave pattern for blunt-nose and sharp wedges demonstrates the principal change in the flow structure at the

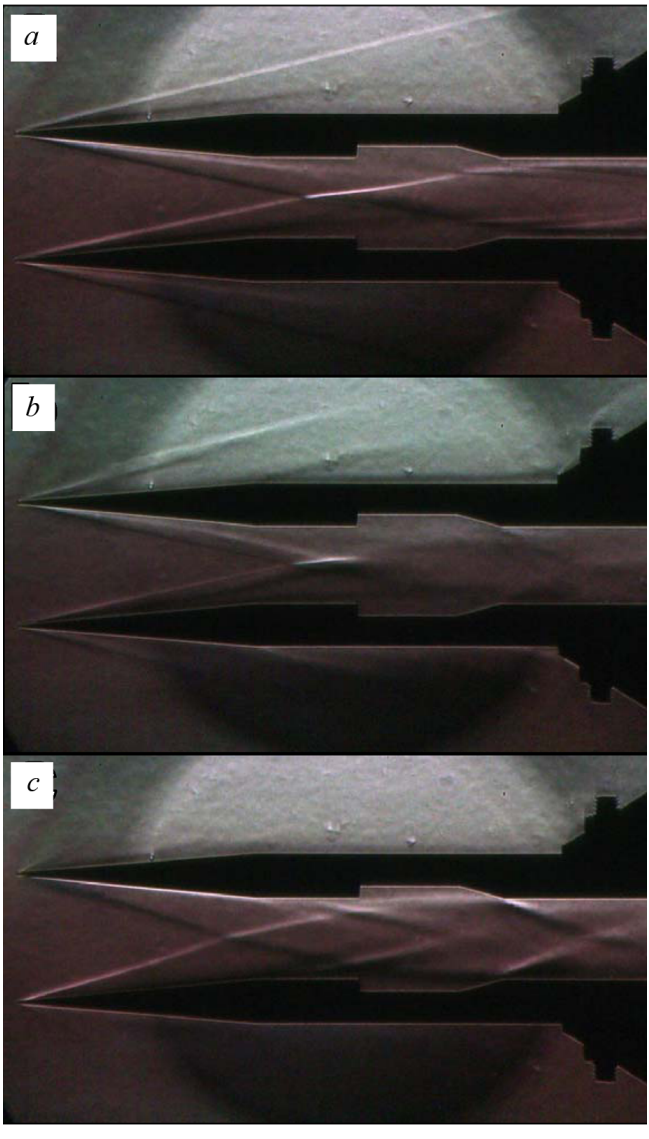

Fig. 6. Shockwave structure formed by the flow around two wedge models

transition from sharp to blunt-nose wedges. It can be observed that of the model gas dynamic passageway was "filled" more rapidly with the higher pressure flow region generated by the shock waves which is caused by the head shock waves formation at the leading blunt-nose edges. From this standpoint the bluntness plays undoubtedly a positive role. It should be also noted that during the interaction of the blunt-nose shock wave with the boundary layer local heating is observed near the surface [1, 12].

Numerical modelling of the flow in the gas dynamic passageway model. Main equations. For the numerical modelling of the gas dynamic processes in the shock tube testing chamber which was described above, let's assume that the flow is described by Navier–Stokes–Fourier equations

for compressible media which are laws of conservation of mass, momentum and energy in viscous gas:

$$\partial_t U + \nabla \cdot \vec{F}^c - \nabla \cdot \vec{F}^v = S$$

under relevant initial and boundary conditions. In these equations vector $U = (\rho, \rho v_1, \rho v_2, \rho v_3, E)^{\mathrm{T}}$is a conservative vector, where ρ is density, E is total energy and $\vec{v} = (v_1, v_2, v_3) \in R^3$ is velocity vector in the cartesian coordinate system; $\vec{F}^c(U)$ are convective currents, $\vec{F}^v(U)$ are viscous currents and $S(U)$ is the generic source component:

$$\vec{F}_i^c = \begin{pmatrix} \rho v_i \\ \rho v_i v_1 + p\delta_{i1} \\ \rho v_i v_2 + p\delta_{i2} \\ \rho v_i v_3 + p\delta_{i3} \\ v_i (E + p) \end{pmatrix}, \; \vec{F}_i^v = \begin{pmatrix} 0 \\ \tau_{i1} \\ \tau_{i2} \\ \tau_{i3} \\ v_j \tau_{ij} + k\partial_i T \end{pmatrix}, \; i = 1, 2, 3,$$

where ρ is static pressure, T is temperature, δ_{ij} is Kronecker symbol and the viscous stress tensor is recorded as $\tau_{ij} = \mu(\partial_j v_i + \partial_i v_j - 2/3\delta_{ij}\nabla \cdot \vec{v})$. It should be noted that i, j indexes denote 3D cartesian coordinates, while repeated indexes denote summation. Calorically perfect gas is used as the operating medium, and the heat capacities ratio γ is assumed to equal 1.4. The molecular viscosity μ is calculated from Sutherland's formula, for the thermal conductivity k the assumption of Prandtl number equalling 0.72 is used.

The numerical method used is a variation of finite volume approach and can be regarded as Godunov's method variation. If the parameters within cells (finite volumes) are assumed to be distributed constantly, the method has only first-order accuracy in space. To achieve second-order accuracy the piecewise linear reconstruction is used [13]. For example, variables vectors leftside and right side the cell dividing the adjacent cells i and j can be defined as follows:

$$q_L = q_i + \nabla q_i \cdot \vec{r}_L,$$

$$q_R = q_j + \nabla q_j \cdot \vec{r}_R,$$

where q is a scalar variable; ∇q is this variable gradient; $\vec{r}$ is the vector passing from the cell centre into the face centre.

Non-viscous flows can be calculated with different variants of the exact or approximate solution of Riemann problem. In the software used most of the popular solvers are realized. This research used AUSM (advective upstream splitting method) [14]. This approach to non-viscous flow calculation is quite economical and suitable for viscous flows calculation.

The gradients for linear reconstruction can be calculated either from Green-Gauss theorem, either with the least squares method. Green-Gauss theorem [13] can be used to obtain the precise value of the linear function gradient only for tetraedrical cells, and thus is not applicable for non structured nets with different shape cells. Consequently in this research the weighted least squares method is used by default for reconstruction.

It is well-known that second- or higher order reconstruction require limiters to suppress false oscillations of the solution in the large gradients area. The software in question employs Barth and Jespersen [13], Venkata-Krishnan's [15], Michalak and Ollivier-Gooch [16] limiters.

Speed and temperature gradients at the cell faces for viscous flows are calculated as the mean value of the gradients in the cells centres with Green–Gauss theorem or with the least squares method described above:

$$\nabla q_{ij} \cdot \vec{n} = \frac{1}{2} \left(\nabla q_i + \nabla q_j \right) \cdot \vec{n}.$$

However in [17] it was demonstrated that this approach can result in the discoordination of the solution for quadrangular or hexagonal meshes. The following modified formula[18] is applied to reduce the method discoordination error:

$$\nabla q_{ij} \cdot \vec{n} = \frac{q_j - q_i}{\|\vec{r}_j - \vec{r}_i\|} \alpha_{ij} + \frac{1}{2} \left(\nabla q_i + \nabla q_j \right) \cdot \left(\vec{n} - \alpha_{ij} \vec{s} \right),$$

where$\vec{n}$ is the normal to the cell face; $\vec{s}$ is the normalised vector connecting cells centres; $\|\vec{r}_j - \vec{r}_i\|$is the distance between i and j cells centres; α_{ij} is the scalar product $\alpha_{ij} = \vec{s} \cdot \vec{n}$. We should remind that ∇q_i gradient in i cell is calculated either with Green-Gauss theorem, either with the smallest squares approach.

For the time discretization explicit Runge–Kutta methods of the second- or third-order accuracy [19] can be used. The time step can be calculated with regard to non-viscous and viscous limits to the step size.

Numerical modelling results for the gas dynamic duct flow. Comparison with the experiment. Numerical investigation was performed according to a previously designed approach for two aerodynamic models which were experimantally investigated in a two-membrane aerodynamic shock tube at Institute for Problems in Mechanics of RAS. During the numerical simulation the flow in the test chamber was viewed separately from the shockwave motion in the shock tube starting at a short distance from the nozzle. It is assumed that the receiver walls do not affect the flow near the model. In this research it is also assumed that the flow after the nozzle section is uniform in the lateral direction (the uniformity issues of

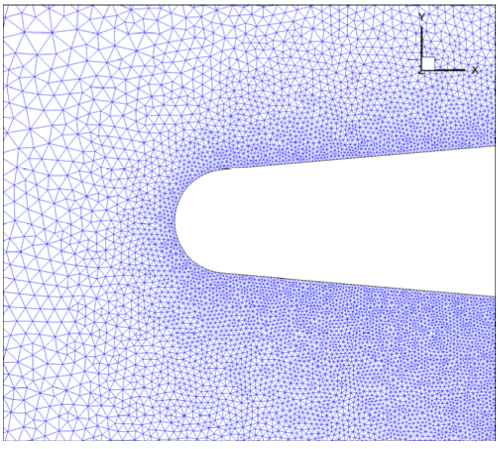

Рис. 7. The leading edge of the blunt-nose wedge, computation mesh detail

the ram air in the lateral direction are presented in [10]). The Mach number of the ram air is estimated from the experimental data using the angle of the shockwave leaving the wedge in photos corresponding to the quasi steady flow modes. As a result the input parameters at the inflow boundary in the numerical simulation are the following: M = 7.0 or 4.5 (two quasi steady modes were regarded); the temperature is 100 K; viscousity coefficient is equal to the air viscousity coefficient at the entry temperature.

For two model gas dynamic ducts (with sharp and blunt-nose edges) two different meshes are created. These sets are three-dimensional in design, they contain only one layer of cells in Z axis direction, so these meshes will be regarded as two-dimensional. The mesh for the sharp-edge model contains 363 500 triangular or quandrangular cells with a minimal cell size of $2 \cdot 10^{-4}$ near hard surfaces. The Gmsh generator [20] was used to create the mesh.

The enthropy layers generated near the decelerating point of the blunted body can significantly affect the flow inside the ramjet air intake, so these layers should have a good resolution. The resolution must be especially high near the blunt-nose wedge leading edge. The mesh for the blunted edge contains 1 200 000 cells with the minimal cell size of 0.01 mm near the hard walls. Fig. 7 shows details of the mesh for the blunt-nose model near the wedge leading edge.

All calculations were done in a complete calculation field without any assumptions on the flow symmetry. On the one side it was used as an additional verification of the solution quality, on the other hand furher research is planned on the effects of the entry current non-uniform patters and a small angle of attack.

The least squares method [13] with Michalak and Ollivier–Gooch limiters [16] was used to calculate the physical variables gradients in the cells centres. The calculations were done with Runge-Kutta second-order method [19] with Courant number of 0.5.

The comparison of the calculation results with the experimental data is presented in Fig. 8, 9. The upper part of each figure contains the Shlieren image from the test, and the lower part — isolines of the calculated density

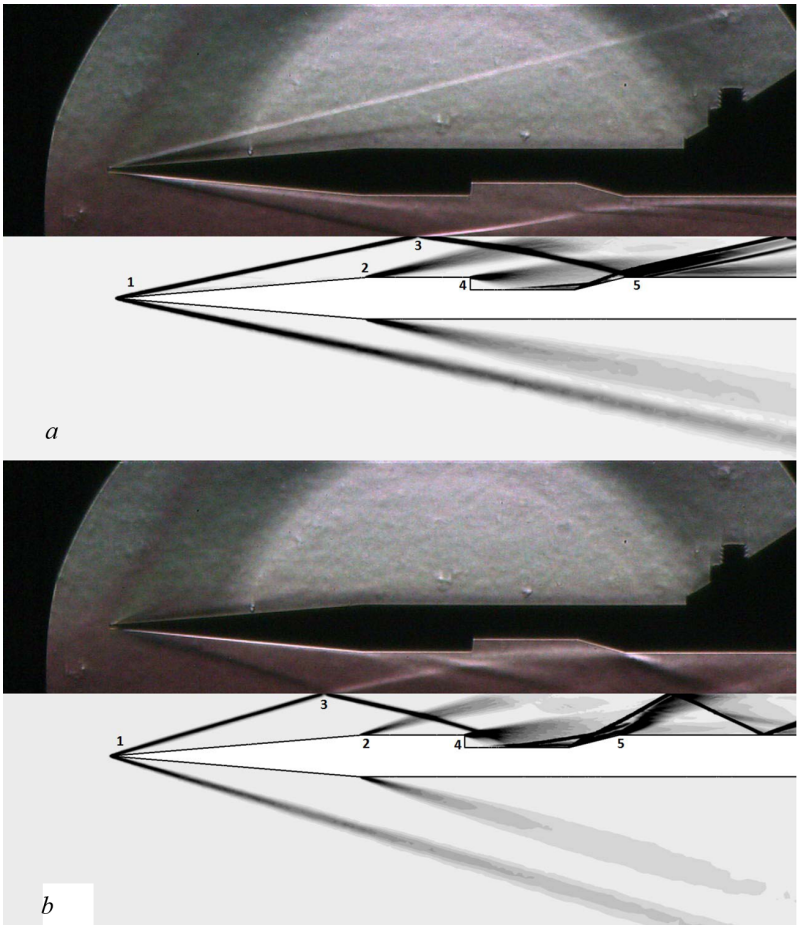

Fig. 8. Comparison of the experiment and the calculation of the ramjet sharp edge model at $M = 7.0$ (*a*) and $M = 4.5$ (*b*)

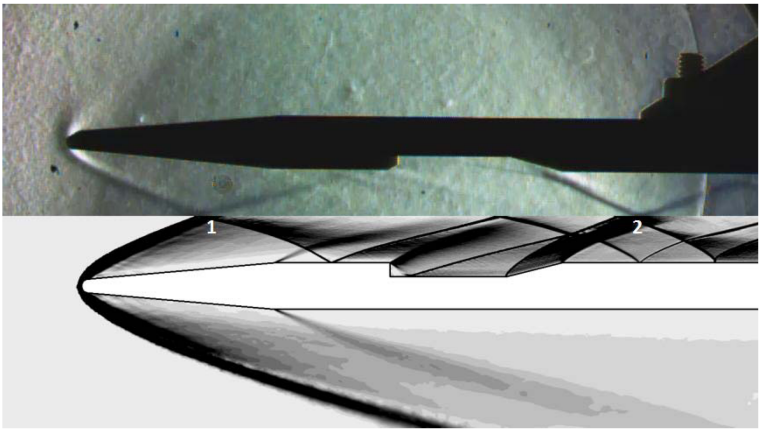

Fig. 9. Experiment and computation comparison for the blunt-nose ramjet model at $M = 7.0$

gradient module. A reverse range of greys was used when creating isolines to enable better comparison.

The first quasi steady stage of the sharp edge model flow is presented in Fig. 8. The numerical modelling was performed for the $M = 7$ of the ram air. In area *1* (Fig. 8 *a*) the attached shock wave front is clearly visible which can also be observed in the Schlieren image. In the transition location of the wedge angular surface (area *2*, Fig. 8 *a*) rare faction waves fan is observed which is not so visible in the shadow image, it can be the result of the boundary layer and separation flows in this area affecting the shadow image. In the area *3* (Fig. 8 *a*) the attached shock wave fronts intersection is visible, which can denote the good level of validation for the approach flow. Near the initial step of the cavity (Fig. 8 *a*, area *4*) a series of rare faction waves is visible, whose outline is also present in the experiment data. At the end of the cavity (Fig. 8 *a*, area *5*) a complex structure of rarefaction waves is formed, which coincides in some respects with the shadow image.

The comparison of the experiment Schlieren image with the numerical simulation results for the second quasi steady sharp-edge flow stage is presented in Fig. 8 *b*, which shows that the high density gradient areas (areas *1–4*, Fig. 8 *b*) are in good agreement. The comparison results of the flow after the cavity (area *5*, Fig. 8 *b*) have also visibly improved, which may be the consequence of a lower Mach number simulation of the approach flow and correspondingly more peaked fronts of the wave structure observed.

The experiment image of the first quasi steady blunt-nose flow stage is compared to the numerical simulation results in Fig. 9. The experiment image quality is lower than the one with the sharp edge because the video camera used had smaller resolution. In the case of the blunt nose wedge, the detached shock wave (area *1*, Fig. 9) and rare faction waves (area *2*, Fig. 9) fronts have more blurred boundaries. However, the comparison of flow structure in this area indicates that the numerical solution adequately corresponds to the experiment. The majority of density field characteristics present in the experiment photo image can be observed on the isolines of the calculated density gradient. It should be noted that the comparison of Fig. 8 *a* and Fig. 9 leads to the conclusion that the blunt edge flow is somewhat more complicated than sharp edge flow.

Conclusion. The flow structure for the air intake and ramjet passage models was investigated experimentally and numerically in “Radiative gas dynamics” laboratory in the Institute for Problems in Mechanics of RAS. The change of cold air flows with $M = 7$ and 4.5 around sharp and blunt nose wedge models was recorded with high speed video cameras. The experiment results are used to test numerical simulation of shockwave

processes and gas dynamic effects. The resolution of the numerical results is significantly higher, thus the flow can be investigated in more detail.

The research was conducted in the framework of the Russian Federation President's grant MK-5324.2014.1 in support of young Russian scientists.

REFERENCES

[1] Borovoy V.Ya., Egorov I.V., Noev A.Yu. Two-dimensional interaction of falling shock wave with turbulent boundary layer in presence of entropy layer. *Mekhanika zhidkosti i gaza* [Fluid Dynamics], 2011, no. 6, pp. 88–109. (in Russ.).

[2] Gerasimov S.I., Faykov Yu.I., Kholik S.A. Kumulyativnye istochniki sveta [Cumulative light sources]. Sarov, FGUP "RFYaTs-VNIIEF" Publ., 2011. 327 p.

[3] Gerasimov S.I., Faykov Yu.I. Tenevoe fotografirovanie v raskhodyashchemsya puchke sveta [Shadow photography in divergent light beam]. Sarov, FGUP "RFYaTs-VNIIEF", 2010. 344 p. (in Russ.).

[4] Kovalev P.I., Mende N.P., eds. Al'bom sverkhzvukovykh techeniy [Catalogue of supersonic flows]. SPb., Politekh. un-t Publ., 2011. 251 p.

[5] Krasnov I.F., Koshevoy V.N., Danilov A.N. Prikladnaya aerodinamika [Applied aerodynamics]. Moscow, Vyssh. shk. Publ., 1974. 732 p.

[6] Zvegintsev V.I. Gazodinamicheskie ustanovki kratkovremennogo deystviya. Ch. 1. Ustanovki dlya nauchnykh issledovaniy [Short-term gas-dynamic devices. Part 1]. Novosibirsk, Parallel' Publ., 2014. 551 p.

[7] Kotov M.A., Ruleva L.B., Solodovnikov S.I., Surzhikov S.T. Experimental research of the model flow-over in hypersonic aerodynamic shock tube. 5-ya Vseross. shk.-seminar "Aerofizika i fizicheskaya mekhanika klassicheskikh i kvantovykh sistem". *Sb. Nauch. Tr.* [5th All-Russian School-Seminar "Aerophysics and Physical Mechanics of Classical and Quantum Systems": Proc. Sci. Int.]. Moscow, IPMekh RAN, 2012, pp. 110–115 (in Russ.).

[8] Kotov M.A., Kuzenov V.V. Main trends in research of hypersonic flows in aerodynamic shock tubes. *Izobretatel'stvo*, 2013, vol. XIII, no. 9, pp. 11–25 (in Russ.).

[9] Kotov M.A., Kryukov I.A., Ruleva L.B., Solodovnikov S.I., Surzhikov S.T. Experimental Investigation of an Aerodynamic Flow of Geometrical Models in Hypersonic Aerodynamic Shock Tube. AIAA 2013-2931. *AIAA Wind Tunnel and Flight Testing Aero II*. 15 p.

[10] Kotov M.A., Kryukov I.A., Ruleva L.B., Solodovnikov S.I., Surzhikov S.T. Multiple Flow Regimes in a Single Hypersonic Shock Tube Experiment. AIAA 2014-2657. *AIAA Aerodynamic Measurement Technology and Ground Testing Conference*. 22 p.

[11] Gruber M.R., Baurle R.A., Mathur T., Hsu K.-Y. Fundamental Studies of Cavity-Based Flame holder Concepts for Supersonic Combustors. *J. of Propulsion and Power*, vol. 17, no. 1, 2001, pp. 146-153.

[12] Borovoy V.Ya. Techenie gaza i teploobmen v zonakh vzaimodeystviya udarnykh voln s pogranichnym sloem [Gas flow and heat exchange in interaction areas of shock waves with boundary layer]. Moscow, Mashinostroenie Publ., 1983. 141 p.

[13] Barth T.J., Jespersen D.C. The design and application of upwind schemes on unstructured meshes. *AIAA Paper*, No. 1989-0366, June 1989.

[14] Liou M.S., Steffen C.J.Jr. A New Flux Splitting Scheme. *J. of Computational Physics*, 1993, vol. 107, pp. 23–39.

[15] Venkatakrishnan V. Convergence to Steady State Solutions of the Euler Equations on Unstructured Grids with Limiters. *J. of Computational Physics*, 1995, vol. 118, pp. 120–130.

[16] Michalak C., Ollivier-Gooch C. Accuracy preserving limiter for the high-order accurate solution of the Euler equations. *J. of Computational Physics*, 2012, vol. 228, pp. 8693–9711.
[17] Haselbacher A., Blazek J. Accurate and efficient discretization of Navier–Stokes equations on mixed grids. *AIAA J.*, 2000, vol. 38, no. 11, pp. 2094–2102.
[18] Weiss J.M., Maruszewski J.P., Smith W.A. Implicit solution of preconditioned Navier–Stokes equations using algebraic multigrid. *AIAA J.*, 1999, vol. 37, no. 1, pp. 29–36.
[19] Shu C.-W., Osher S. Efficient Implementation of Essentially Non-Oscillatory Shock-Capturing Schemes II. *J. of Computational Physics*, 1989, vol. 83, pp. 32–78.
[20] Geuzaine C., Remacle J.-F. Gmsh: a three-dimensional finite element mesh generator with built-in pre- and post-processing facilities. *International J. for Numerical Methods in Engineering*, 2009, vol. 79, no. 11, pp. 1309–1331.

Contributors

Kotov M.A. — Research Fellow, Laboratory of Radiation Gas Dynamics, Institute for Problems in Mechanics of RAS, author of 18 research publications in the field of aerothermophysics.
Institute for Problems in Mechanics of the Russian Academy of Science, Vernadskiy prospect 101, building 1, Moscow, 119526 Russian Federation.

Kryukov I.A. — Ph.D. (Phys.-Math.), Senior Research Fellow, Laboratory of Radiation Gas Dynamics, Institute for Problems in Mechanics of RAS, Associate Professor, Department of Physical and Chemical Mechanics, Moscow Institute of Physics and Technology, author of over 90 research publications in the fields of thermal physics and radiation gas dynamics.
Institute for Problems in Mechanics of the Russian Academy of Science, Vernadskiy prospect 101, building 1, Moscow, 119526 Russian Federation.

Ruleva L.B. — Leading Engineer, Laboratory of Radiation Gas Dynamics, Institute for Problems in Mechanics of RAS, author of over 70 publications in the field of aerothermophysics, 20 inventor's certificates in the fields of navigation, automated control, and gas dynamics.
Institute for Problems in Mechanics of the Russian Academy of Science, Vernadskiy prospect 101, building 1, Moscow, 119526 Russian Federation.

Solodovnikov S.I. — Research Scientist, Laboratory of Radiation Gas Dynamics, Institute for Problems in Mechanics of RAS, author of 11 publications in the field of aerothermophysics.
Institute for Problems in Mechanics of the Russian Academy of Science, Vernadskiy prospect 101, building 1, Moscow, 119526 Russian Federation.

Surzhikov S.T. — D.Sc.(Phys.-Math.), Corresponding Member of the Russian Academy of Sciences, Head of Laboratory of Radiation Gas Dynamics, Institute for Problems in Mechanics of RAS. Professor of Physics and Mathematics, Head of the Department of Physical and Chemical Mechanics, Moscow Institute of Physics and Technology, author of over 500 research publications in the fields of thermal physics and radiation gas dynamics.
Institute for Problems in Mechanics of the Russian Academy of Science, Vernadskiy prospect 101, building 1, Moscow, 119526 Russian Federation.

The translation of this article from Russian into English is done by I.N. Shafikova, a senior lecturer in the Chair of English Language, Linguistics Department, Bauman Moscow State Technical University under the general editorship of N.N. Nikolaeva, Ph.D. (Philol.), Associate Professor in the Chair of English Language, Linguistics Department, Bauman Moscow State Technical University.